

SENSITIZED RANS-BASED EULER-LAGRANGE MODELING OF A TURBULENT PARTICLE-LADEN FLOW

Xiaoyu Wang, Jeanette Hussong, Suad Jakirlic

Institute of Fluid Mechanics and Aerodynamics
Technical University of Darmstadt

Peter-Grünberg-Str.10, 64287, Darmstadt, Germany
wang.x@sla.tu-darmstadt.de, jakirlic@sla.tu-darmstadt.de

ABSTRACT

The behavior of small, heavy, spherical particles in turbulent flow occurring in pipe, plane channel, and backward-facing step configurations is currently studied computationally by a multiphase Euler-Lagrange modeling approach employed within a time-accurate, eddy-resolving simulation based on a sensitized Reynolds-Averaged Navier-Stokes (RANS) framework. The dynamics of the unresolved subscale motion in the latter method is described by a transport model based on the solution of the entire fine-structure stress tensor. The scale-resolving capability of this model is achieved by appropriate production enhancement of the length-scale determining dissipation rate, which subsequently causes the fully-modeled RANS turbulence to be reduced to the level of sub-scale structures, in accordance with the so-called scale-adaptive strategy of Menter & Egorov (2010), allowing a corresponding amount of resolved turbulence from flow momentum convection. The underlying formulation of the latter model scheme corresponds to a near-wall Reynolds stress model (RSM, Jakirlic & Maduta (2015)), the baseline version of which was also used for the comparative evaluation. For the turbulent pipe flow, the particle volume fraction is assumed to be sufficiently small that the effects of the particles on the carrier fluid flow (one-way coupling) and particle collisions are considered negligible, as also assumed in the reference Direct Numerical Simulation (DNS) of Portela *et al.* (2002). Particle-turbulence interactions near the wall in a channel flow are studied with a four-way coupling Euler-Lagrange model and compared with the DNS results of Dritselis & Vlachos (2008). Furthermore, the study of feedback particle forces on the fluid in a backward-facing step flow adopts a two-way coupling framework, which is calibrated alongside the experimental observations presented by Fessler & Eaton (1999). The comparative results assessment confirms that the present model using the Euler-Lagrange approach accurately reproduces the properties of particle-laden flows across different flow regimes characterized by variation in Stokes numbers, Reynolds numbers and configuration geometries, as illustrated by the discrepancies in particle-related properties by approaching the wall. Significantly, the characteristic turbulence modulation caused by the presence of particles is reliably captured in the turbulent particle-laden turbulent channel flow configuration.

INTRODUCTION

Turbulent flows characterized by the presence of small heavy particles are prevalent in a wide range of engineering applications and respective scientific studies. These scenarios,

such as the dispersion of pollutants in the atmosphere and the transport of contaminants in industrial applications, are primarily dominated by fluid-particle interactions. In these studies, a two-way coupling framework has been applied to facilitate momentum exchange between the continuous and particulate phases. In addition, when dealing with particle-laden flows with higher particle volume fractions, particle collisions have been considered within a four-way coupling approach to ensure a comprehensive simulation that captures the particle dynamics inherent in such a multiphase system.

However, traditional approaches that utilize the conventional RANS equations, which incorporate various empirical parameterizations in an attempt to represent the full spectrum of velocity fluctuations, are insufficient to accurately capture the complex interactions between particles and turbulence. Accurate prediction of particle transport depends significantly on a realistic description of the time-dependent, three-dimensional velocity field encountered along particle trajectories, see e.g. Berlemont *et al.* (1990) and Simonin *et al.* (1995). Thus, a presently employed eddy-resolving version of the conventional RANS model, designed to represent the subscale structures of turbulence and particle transport in turbulent flows, is considered a powerful tool for providing flow characteristics that are difficult to extract using conventional RANS-related prediction tools.

COMPUTATIONAL MODEL Eulerian framework

The carrier fluid is assumed to be incompressible. Therefore, the momentum equations governing the velocity field within the unsteady conventional and sensitized RANS models read:

$$\frac{\partial U_i}{\partial t} + U_j \frac{\partial U_i}{\partial x_j} = -\frac{1}{\rho} \frac{\partial p}{\partial x_i} + \frac{\partial}{\partial x_j} \left(\nu \frac{\partial U_i}{\partial x_j} - \overline{u_i' u_j'} \right) + \overline{S_m} \quad (1)$$

where the $\overline{S_m}$ represents the momentum exchange source term to account for the particle feedback force per unit mass of fluid. The stress tensor $\overline{u_i' u_j'}$, determined by a differential near-wall second-moment closure model, represents the fully-modeled Reynolds stress tensor in the conventional RANS-RSM approach (Jakirlic & Hanjalic (2002)), i.e. the stress tensor of the unresolved residual fine structures within the sensitized-RANS method (Jakirlic & Maduta (2015)). Within the framework of the latter approach, denoted as the Improved Instability-Sensitive Reynolds Stress Model (IIS-RSM), the

equation of the specific dissipation rate ($\omega^h = \varepsilon^h/k$) is introduced comprising an additional production source formulated in terms of the second derivative of the underlying velocity field ($\nabla^2 U_i$), appropriately designed to adequately capture flow fluctuations to an extent consistent with the resolved turbulence unsteadiness, analogous to the Scale-Adaptive Simulation (SAS) methodology (Menter & Egorov (2010)):

$$\left(\frac{D\omega^h}{Dt}\right)_{IISRSM} = \left(\frac{D\omega^h}{Dt}\right)_{RSM} + P_{IISRSM}, P_{IISRSM} = f(\nabla^2 U_i) \quad (2)$$

For the sake of brevity, the full model specification is not given here; interested readers are referred to Jakirlić & Maduta (2015) and Joksimović *et al.* (2023).

The turbulence model equations are implemented in the second-order accurate finite-volume-based numerical code OpenFOAM®, which was used for all simulations.

Lagrangian particle tracking approach

In the validation scenarios under consideration, the particle transport equation governing the motion of particles with densities considerably greater than that of the carrier fluid and diameters less than the Kolmogorov scale, is given by:

$$m_p \frac{d\mathbf{u}_p}{dt} = \sum \mathbf{F}_i = \mathbf{F}_D + \mathbf{F}_G + \mathbf{F}_L \quad (3)$$

The particle Reynolds number is defined as:

$$Re_p = \frac{\rho_f D_p |\mathbf{u}_f - \mathbf{u}_p|}{\mu_f} \quad (4)$$

with the density ρ_f and the dynamic viscosity μ_f of the fluid or the continuous phase, the particle diameter D_p and the magnitude of the relative slip velocity $|\mathbf{u}_f - \mathbf{u}_p|$. The drag force for a spherical particle is evaluated as:

$$\mathbf{F}_D = C_D \frac{\pi D_p^2}{8} \rho_f (\mathbf{u}_f - \mathbf{u}_p) |\mathbf{u}_f - \mathbf{u}_p| \quad (5)$$

where the drag coefficient is determined by the following drag model based on an empirical correlation according to Putnam (1961):

$$C_D = \begin{cases} \frac{24}{Re_p} \left(1 + \frac{1}{6} Re_p^{2/3}\right) & \text{if } Re_p \leq 1000 \\ 0.424 & \text{if } Re_p > 1000, \end{cases} \quad (6)$$

The gravitational and buoyancy forces are calculated as a total force as follows

$$\mathbf{F}_G = m_p \mathbf{g} \left(1 - \frac{\rho_f}{\rho_p}\right) \quad (7)$$

where \mathbf{g} is the gravitational acceleration vector. The Saffman force arises due to local shear flows forming a non-uniform velocity distribution over the particle surface and could be calculated using the Saffman-Mei model derived by Saffman (1965) and extended by Mei (1992). The lift is based on the shear

Reynolds number, defined as

$$Re_s = \frac{\rho_f D_p^2 |\nabla \times \mathbf{u}_f|}{\mu_f}, \quad (8)$$

which is used to evaluate the coefficients of the Saffman-Mei model:

$$\beta = \frac{1}{2} \frac{Re_s}{Re_p}, \quad \alpha = 0.3314 \sqrt{\beta}, \quad (9)$$

$$f = (1 - \alpha) \exp(-0.1 Re_p) + \alpha. \quad (10)$$

Afterward, the lift coefficient C_{LS} is calculated using the following approximation:

$$C_{LS} = \begin{cases} 6.46f & \text{if } Re_p < 40 \\ 6.46 \cdot 0.0524 \sqrt{\beta} Re_p & \text{if } Re_p \leq 40, \end{cases} \quad (11)$$

The lift coefficient C_L is now formulated as a non-dimensional lift coefficient:

$$C_L = \frac{3}{2\pi \sqrt{Re_s}} C_{LS} \quad (12)$$

Finally, the lift force is calculated as:

$$\mathbf{F}_L = C_L \rho_f \frac{\pi D_p^3}{6} (\mathbf{u}_f - \mathbf{u}_p) \times (\nabla \times \mathbf{u}_f) \quad (13)$$

RESULTS AND DISCUSSION

Flow in a pipe

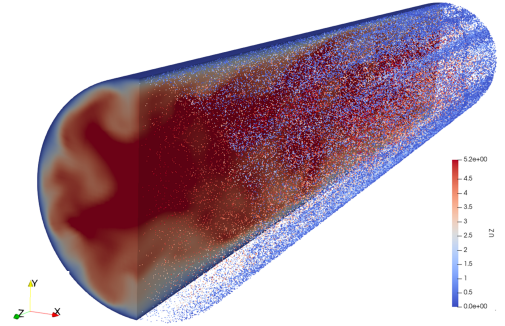


Figure 1: Instantaneous velocity for fluid (left) and particle (right) phases in a particle-laden turbulent pipe flow with $St_b = 1$ obtained by the IIS-RSM

The presently considered flow configuration is a fully-developed turbulent particle-laden pipe flow, illustrated in Fig.1 by visualizing the instantaneous streamwise velocity fields for fluid and particles over the entire computational domain for the case $St_b = 1$. The scale-resolving capability of IIS-RSM in capturing the fluctuating turbulent structures and particle dynamics is clearly evident. The Reynolds number based on the friction velocity $u_\tau = \sqrt{\tau_w/\rho_f}$ and the pipe radius R is $Re_\tau = u_\tau R/\nu = 180$, corresponding to the flow

Reynolds number $Re_b = U_m d / \nu \approx 5300$, where d and U_m are the pipe diameter and the bulk velocity, respectively. Particles with different diameters are treated, corresponding to $St_b = 1$ and $St_b = 4$, where St_b is the bulk Stokes number based on the particle relaxation time τ_p :

$$St_b = \frac{\tau_p U_m}{d} \quad \tau_p = \frac{\rho_p D_p^2}{\rho_f 18\nu} \quad (14)$$

The computational domain for the pipe flow simulation was $5d \times 2\pi \times d$ in the streamwise, circumferential, and radial directions, respectively, with a corresponding grid cell arrangement resulting in a resolution of $120 \times 144 \times 65$ cells. A uniform grid spacing was used in the streamwise and circumferential directions, while a non-uniform grid, appropriately refined toward the wall, was used in the radial direction, with the first grid point located well below $y^+ < 1$. No-slip boundary conditions are applied at the walls, and periodic boundary conditions are applied in the streamwise directions. The simulations are initialized without the presence of particles. After reaching a statistically steady flow state, the particles were introduced at random spatial positions, each with an initial velocity of zero. Apart from the difference in particle diameter, the operating conditions of the two cases remain identical. The relevant particle parameters for the two cases are given in Table 1. The superscript $+$ serves as a notation for the variable normalization using wall units with wall shear velocity u_τ and kinematic viscosity coefficient ν . The particle/fluid density ratio is constant for both cases at $\rho_p/\rho_f = 1000$. The number of particles corresponds to $N_p = 1.5 \times 10^5$.

Table 1: Particle parameters

Case	St_b	τ_p^+	d_p/d	d_p^+
1	1	26	1.8×10^{-3}	0.66
2	4	104	3.7×10^{-3}	1.36

Prior to the quantitative evaluation of the particle-related quantities, it is important to assess the accuracy of the adopted turbulence models with respect to the single-phase flow dynamics. Accordingly, Fig.2 shows a comparison of the semi-logarithmic profiles of the non-dimensional streamwise velocity and turbulence intensity components obtained by both the conventional RSM and the IIS-RSM against the DNS reference data. Except for some underprediction of the velocity in the logarithmic and outer flow region with respect to the conventional RSM, the results of both models closely follow the DNS data. While the profiles obtained by the conventional RSM show reasonable discrepancies compared to the reference DNS, the turbulence intensities captured by the IIS-RSM show very good agreement with the DNS results, except for a slight overprediction in the viscosity-affected near-wall region. In summary, the IIS-RSM related results show a remarkable quantitative agreement with the DNS data, thus demonstrating a high potential to accurately provide the underlying turbulence statistics, which is essential for the correct determination of the particle dynamics.

After a statistically steady particle concentration was achieved, particle-related results were evaluated by averaging the instantaneous fields over the pipe cross-section and time.

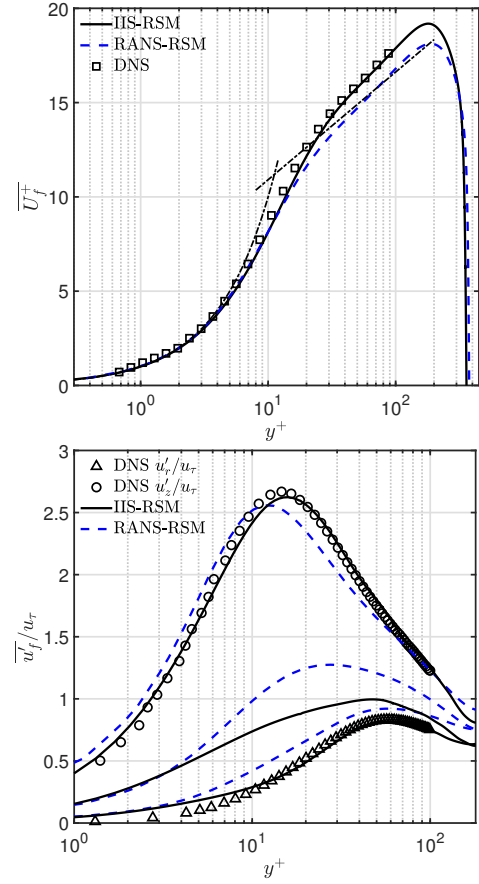


Figure 2: Semi-logarithmic profiles of mean fluid velocity (upper) and turbulence intensities (lower) for the particle-free pipe flow.

Fig.3 shows the mean streamwise velocity profiles for particles with different St_b numbers, along with the single-phase fluid velocity predicted by IISRSM. In both cases, the mean particle velocities predicted by the present Euler-Lagrange approach are in good agreement with the DNS data, being correspondingly smaller than the mean fluid velocity. Furthermore, the more pronounced effect of the downward shift of the particle velocity relative to the fluid velocity in the case of heavier particles, characterized by $St_b = 4$, is captured correctly.

The profiles of the mean radial and streamwise turbulence intensity components for both the fluid and the particles are shown in Fig.4. The radial turbulence intensity is critical for accurately predicting the particle dynamics in the near wall region. While the turbulence intensities for the particle-free flow show a slight overprediction within the viscous sublayer, the particle-laden flow profiles are in close agreement with the benchmark data for both investigated Stokes numbers. The attenuation of the particle-induced radial velocity fluctuations relative to the continuous phase reflects the particle inertia, which is manifested by a reduced radial turbulence intensity at higher Stokes numbers. Conversely, the tendency of the streamwise turbulence intensity component for the fluid and particles is opposite: particle turbulence intensities are slightly higher than those of the fluid phase. Compared to the DNS data, the profiles obtained by the present Euler-Lagrange approach show a slight overprediction in the region $y^+ < 5$, i.e. in the viscous sublayer.

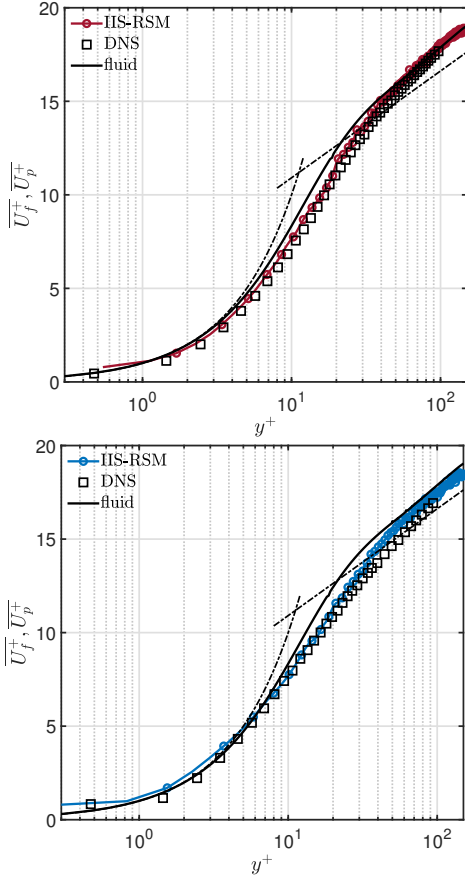


Figure 3: Semi-logarithmic profiles of mean particle velocities with $St_b = 1$ (upper) and $St_b = 4$ (lower)

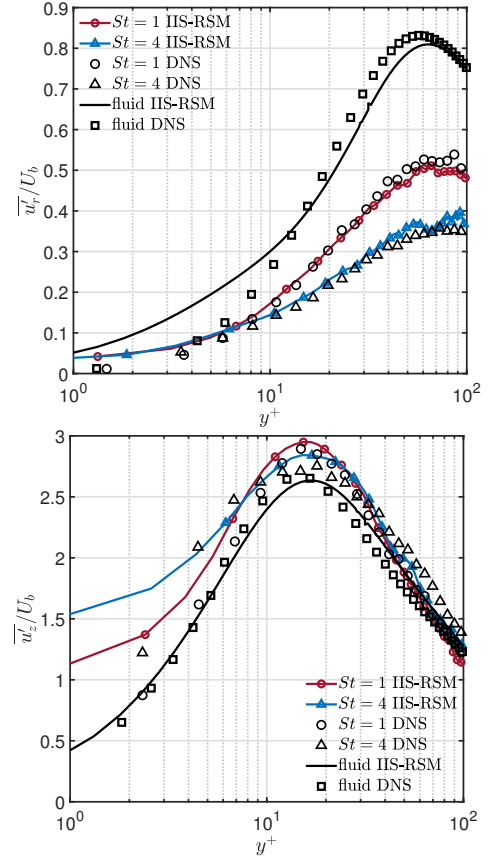


Figure 4: Mean radial (upper) and streamwise (lower) turbulence intensity profiles for the fluid and particles

Flow in a plane channel

Fig. 5 illustrates the particle-laden turbulent flow in a plane channel. The Reynolds number of the particle-free flow, denoted as $Re_b = 5600$, is determined based on the bulk velocity and the channel width h , corresponding to $Re_\tau = 176$ and $Re_\tau = 168$ for the particle-free and particle-laden cases, respectively, based on the friction velocity and the channel half height. This specification is consistent with the reference DNS study conducted by Dritselis & Vlachos (2008). The mass loading ratio of the particles is $\phi_m = 0.5$. The particle diameter is smaller than the Kolmogorov length and the grid spacing, with the latter refined to ensure adequate resolution of the fluid flow scales. The feedback effect of the particles on the fluid phase is considered by a point-force model. Interactions involving both interparticle and particle-wall purely elastic collisions are modeled using the spring-slider-dashpot model proposed by Tsuji *et al.* (1992), thus employing a four-way coupling methodology. For this analysis, the drag force is the only force considered for evaluating the particle dynamics. Particles leaving the computational domain in the downstream or spanwise directions are reintroduced at the corresponding opposite boundaries to ensure flow continuity and dynamics consistency.

For simulations dealing with both particle-free and particle-laden cases, a computational grid consisting of $128 \times 128 \times 128$ points in the x , y and z directions, respectively, was used within a computational domain of size $2\pi h \times 2h \times 2/3\pi h$. The grid spacing was uniform in the periodic streamwise and spanwise directions. A suitable grid grading was implemented in the wall-normal y direction, with the first grid point located well into the viscous sublayer at $y^+ < 1$ for both the particle-

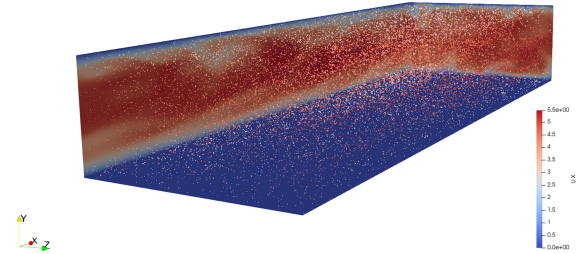


Figure 5: Instantaneous velocity for fluid (at flow domain boundaries) and particle phases in a particle-laden turbulent flow with $St_b = 1$ obtained by the IIS-RSM

free and particle-laden cases. The particles were simulated with a density ratio of $\rho_r = 7333$, corresponding to copper particles suspended in air. The Stokes number based on the centerline Kolmogorov time scale was about $St = 20$.

Fig. 6 shows the mean streamwise velocity profiles for both fluid and particle phases in particle-free and particle-laden flow configurations, which are in good agreement with the DNS reference data. The introduction of particles into the flow does not significantly modify the fluid velocity profile, with only a slight increase in the core region due to the reduced friction velocity under the mass loading condition of $\phi_m = 0.5$. As shown in the lower figure 6, the mean particle stream velocity in the buffer layer is slightly underpredicted compared to the DNS data. However, the large mean slip velocity near the wall is accurately captured, successfully validating the effective implementation of interparticle collision dynamics within the present Euler-Lagrange framework.

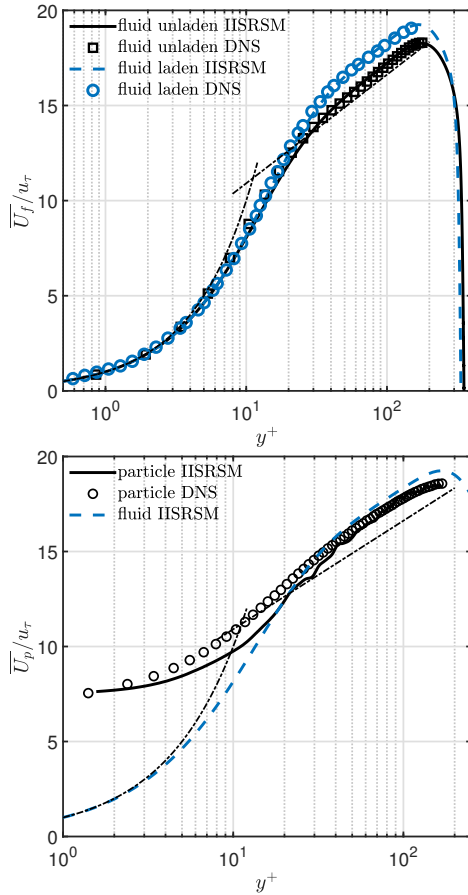


Figure 6: Mean streamwise velocity of fluid phase (upper) and particle phase (lower)

Flow over a backward-facing step

The flow over a backward-facing step, characterized by sharp-edged boundary layer separation and reattachment, is recognized as a suitable benchmark for evaluating the predictive capabilities of turbulence models in the computation of dispersed multiphase flows. Consequently, this recirculating flow configuration is chosen to further evaluate the present Euler-Lagrange approach within the IIS-RSM modeling framework, through comparison with the Laser Doppler Anemometry (LDA) measurements of Fessler & Eaton (1999).

The computational domain is configured in accordance with the experimental setup of Fessler and Eaton, with step and entrance channel heights of $H = 0.0267m$ and $h = 0.04m$, respectively, yielding an expansion ratio of $h/H = 5/3$ as shown in Fig.7. The upstream and downstream channel lengths are set to $L_U = 10h$ and $L_D = 35h$, respectively, with a channel span width of $B = 4.28h$. To ensure a fully-developed inflow condition, a recycling method based on the relatively long upstream channel is employed, in which the turbulent velocity is transferred from a downstream plane back to the inlet. Periodic boundary conditions were applied in the spanwise direction, supplemented by no-slip conditions on the lower and upper walls. The structured grid uses a total of 3.5×10^6 cells, with the wall-adjacent grid point positioned within the viscous sublayer at $y^+ < 1$ by appropriately refining the grid spacing in the wall normal direction. The Reynolds number based on the centerline velocity of the upstream channel and the step height is $Re = u_0 H / \nu = 18700$. Furthermore, spherical monodisperse copper particles with a diameter of $D_p = 70\mu m$ and a density of $\rho_p = 8800kg/m^3$ are randomly introduced at the flow inlet. Thus, the Stokes number, formulated based on the

large-eddy passing frequency in the separated shear layer, is $St = \rho_p D_p^2 u_0 / 10 \mu_f 5H = 6.9$ according to Fessler & Eaton (1999). The particles are injected with a mass loading ratio of $\Phi_m = m_p / m_f$, corresponding to a volume fraction of $\phi_p < 10^{-3}$. Therefore, the flow can be treated as dilute, which allows a two-way coupling approach without considering the interparticle collisions. Consequently, all pertinent forces, including drag, gravity, and Saffman-Mei lift forces, are considered to accurately assess the particle dispersion.

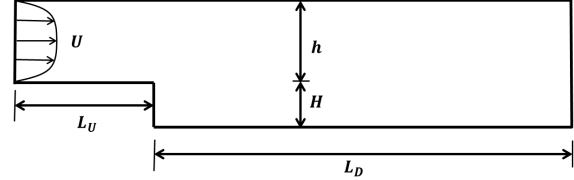


Figure 7: Backward-facing step flow: solution domain

A first impression of the turbulent particle-laden backward-facing step flow can be obtained from Fig. 8, which illustrates the instantaneous streamwise velocity field and particle distribution obtained by the IIS-RSM. The mean streamwise velocity field and associated streamlines are shown in Fig.9, highlighting the recirculation region around the step. As the fully-developed inflow passes the step and undergoes a sudden expansion, it detaches from the sharp edge and reattaches to the lower wall at the length just above $7H$, leading to the formation of a characteristic separation zone.

A quantitative check of the prediction quality of the mean streamwise velocity is presented in Fig.10, with its profile evolution including the separation, reattachment, and post-reattachment regions in the particle-free case. The velocity profiles obtained by both Reynolds stress models agree well with the experimental data, with a very slight overprediction in the upper region of the channel for the IIS-RSM-related results. Both models successfully capture the recirculation zone downstream of the step, correctly returning the experimentally determined reattachment location at $x/H \approx 7.4$.

Fig. 11 shows the time-averaged particle streamwise velocity profiles obtained by the present Euler-Lagrange approach in comparison with the measurement data. It can be seen that the particles mainly follow the fluid flow, as expected from the value of the Stokes number $St = 6.9$. Therefore, the magnitude and skewness of the mean particle velocity profiles are consistent with those of the continuous phase. However, a slight underprediction of the velocity gradient is observed in the region of higher mean shear compared to the experimental data. The deviation decreases progressively as the particles disperse further from the step. The accurate reproduction of the particle distribution in terms of their dispersion characteristics is considered to be a key achievement, demonstrating that there is no need to implement an additional stochastic dispersion model for the present Euler-Lagrange approach.

CONCLUSION

A multiphase Euler-Lagrange computational approach for the prediction of particle-laden flow, implemented within the framework of a Sensitized RANS modeling strategy, describing the dynamics of the entire stress tensor of unresolved turbulence structures, is presented and validated in a series of suitably adopted flow configurations underlying the one-, two-, and four-way coupling between the carrier and dispersed phases. The latter flow characteristics are consistent with operating flow and particle conditions over the range of Reynolds and Stokes numbers considered. The particle-related properties are captured in good agreement with the reference numer-

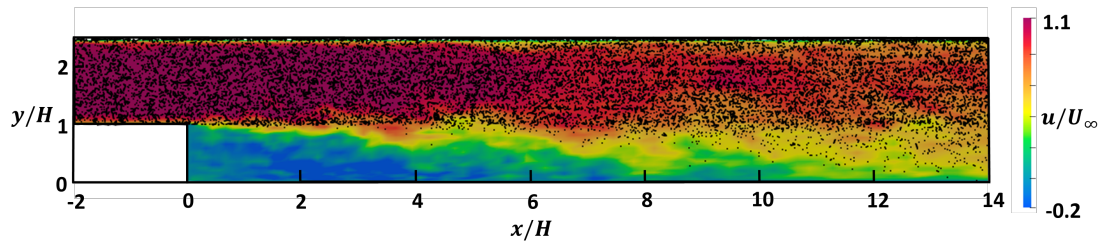


Figure 8: Instantaneous streamwise velocity and particle distribution of the particle-laden turbulent backward-facing step flow obtained by the present IIS-RSM; only 10% of the total particle amount is shown for clarity

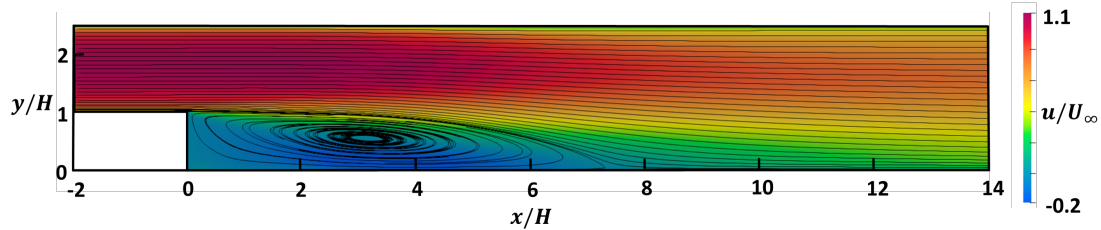


Figure 9: Mean streamwise velocity and associated streamlines for the backward-facing step flow obtained by IIS-RSM

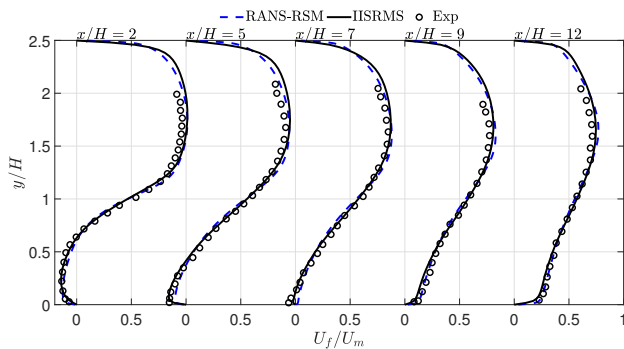


Figure 10: Mean fluid velocity profiles of the particle-free backward-facing step flow

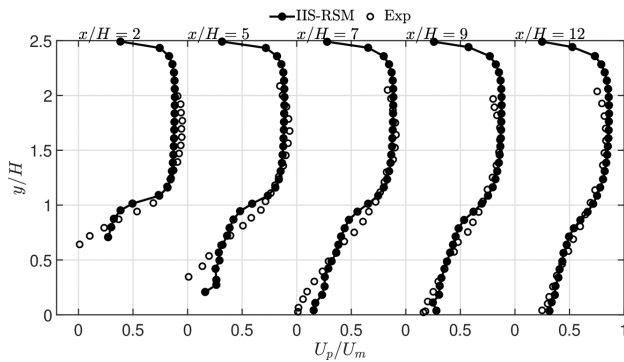


Figure 11: Mean particle velocity of the particle-laden backward-facing step flow

ical and experimental data due to the accurate prediction of the underlying turbulence field. The present Euler-Lagrange multiphase flow approach coupled with the eddy resolving IIS-RSM for turbulence description demonstrates the high potential to correctly capture the fluid-particle interaction in the wall-bounded particle-laden flows.

Acknowledgment. The authors gratefully acknowledge the German Federal Ministry of Education and Research (BMBF) and the federal state of Hessen for supporting this project as part of the NHR4CES (National High Performance Computing Center for Computational Engineering Sciences) funding at TU Darmstadt and RWTH Aachen. The authors furthermore acknowledge the computing time granted on the Lichtenberg High Performance Computer of the Technical University of Darmstadt.

REFERENCES

- Berlemont, A., Desjonqueres, P. & Gouesbet, G. 1990 Particle Lagrangian simulation in turbulent flows. *International Journal of Multiphase Flow* **16** (1), 19–34.
- Dritselis, Chris D. & Vlachos, Nicholas S. 2008 Numerical study of educed coherent structures in the near-wall region of a particle-laden channel flow. *Physics of Fluids* **20** (5), 055103.
- Fessler, John R. & Eaton, John K. 1999 Turbulence modification by particles in a backward-facing step flow. *Journal of Fluid Mechanics* **394**, 97–117.
- Jakirlic, S. & Hanjalic, K. 2002 A new approach to modelling near-wall turbulence energy and stress dissipation. *Journal of Fluid Mechanics* **459**, 139–166.
- Jakirlic, S. & Maduta, R. 2015 Extending the bounds of 'steady' RANS closures: Toward an instability-sensitive Reynolds stress model. *Int. J. Heat and Fluid Flow* **51**, 175–194.
- Joksimović, I., Čorbo, T., Hussong, J. & Jakirlic, S. 2023 Secondary flow and thermal field dynamics in a T-junction with an upstream elbow: a POD-aided, eddy-sensitized Reynolds-stress modeling study. *Int. J. Heat and Fluid Flow* **104**, 109226.
- Mei, R. 1992 An approximate expression for the shear lift force on a spherical particle at finite Reynolds number. *International Journal of Multiphase Flow* **18** (1), 145–147.
- Menter, F. & Egorov, Y. 2010 The scale-adaptive simulation method for unsteady turbulent flow predictions. part I: Theory and model description. *Flow Turbulence and Combustion* **85**, 113–138.
- Portela, Luis M., Cota, Pierpaolo & Oliemans, René V.A. 2002 Numerical study of the near-wall behaviour of particles in turbulent pipe flows. *Powder Technology* **125** (2), 149–157.
- Putnam, A. 1961 Integrable form of droplet coefficient. *ARS Journal* **31**, 1467–1470.
- Saffman, P. G. 1965 The lift on a small sphere in a slow shear flow. *Journal of Fluid Mechanics* **22** (2), 385–400.
- Simonin, O., Deutsch, E. & Boivin, M. 1995 Large eddy simulation and second-moment closure model of particle fluctuating motion in two-phase turbulent shear flows. In *Turbulent Shear Flows 9*, pp. 85–115.
- Tsuji, Y., Tanaka, T. & Ishida, T. 1992 Lagrangian numerical simulation of plug flow of cohesionless particles in a horizontal pipe. *Powder Technology* **71** (3), 239–250.